*Journal of Physiology* (1992), **450**, *pp.* 437–453
*With* 11 *figures*
*Printed in Great Britain*



# $Ca^{2+}$ CURRENT IN MYOTOME CELLS OF THE LANCELET (*BRANCHIOSTOMA LANCEOLATUM*)

BY R. BENTERBUSCH AND W. MELZER*

*From the Lehrstuhl für Zellphysiologie, Ruhr-Universität Bochum, ND-4 D-4630 Bochum, FRG*

(*Received 18 July 1991*)

SUMMARY

1. By using the whole-cell patch clamp method $Ca^{2+}$ and $Ba^{2+}$ currents were measured in the extremely thin twitch muscle cells of the protochordate *Branchiostoma lanceolatum* whose $Ca^{2+}$ channels are likely to resemble the evolutionary ancestors of those found in vertebrate skeletal muscle.

2. When using 10 mM-$Ca^{2+}$ in the artificial external solution and 1 mM-EGTA in the internal solution two kinetically different $Ca^{2+}$ inward current components could be observed, showing very similar voltage dependence of activation and inactivation.

3. In solutions containing 10 mM-$Ba^{2+}$ as an external charge carrier the biphasic inward current turned into a single rapidly activated and slowly inactivating current.

4. Inspecting peak currents, the voltage dependence of fractional activation and inactivation was nearly the same in $Ca^{2+}$ and in $Ba^{2+}$.

5. A transformation into a single component of the $Ca^{2+}$ current could also be observed after perfusing the intracellular lumen with 10 mM of either EGTA or BAPTA. In the case of EGTA this transformation required considerably more time. Probably a higher internal concentration of EGTA is necessary since it binds $Ca^{2+}$ more slowly than BAPTA.

6. Soon after establishing the whole-cell configuration a gradual increase of the second, slow inward current phase was observed relative to the fast component, indicating an enhancement of the slow component by intermediate intracellular buffer concentrations.

7. We conclude that the *Branchiostoma* myotome cells have only one $Ca^{2+}$ channel system. The biphasic appearance of the inward current is caused by an unusually rapid inactivation due to $Ca^{2+}$ ions, which enter the myoplasm during the current and temporarily bind to an inactivation site at the channel. The second phase probably reflects reactivation from the inactivated state upon dissociation of $Ca^{2+}$ from the binding site.

## INTRODUCTION

In skeletal muscle $Ca^{2+}$ release from the sarcoplasmic reticulum (SR) is controlled by voltage-activated $Ca^{2+}$ channels or $Ca^{2+}$-channel-like proteins in the transverse

* To whom all correspondence and reprint requests should be sent.

MS 9564

tubular system (T-system) (Bean, 1986; Ashley, Mulligan & Lea, 1991; Lamb, 1991; Rios & Pizarro, 1991). The present investigation deals with $Ca^{2+}$ channels in twitch muscles of the lancelet (*Branchiostoma lanceolatum*), an organism which is believed to represent a stage of evolutionary development prior to the vertebrates (Franz, 1927). Our work on this preparation aims at gaining insight into the evolutionary roots of the vertebrate $Ca^{2+}$ channels and their involvement in excitation–contraction (E–C) coupling.

The thin (1–2 $\mu$m) muscle cells of *Branchiostoma*, which contain only a thin layer of myofibrils and virtually no T-system (Flood, 1968; Grocki, 1982), were originally believed to become exclusively activated by a $Ca^{2+}$ influx during the action potential (Hagiwara, Henkart & Kidokoro, 1971). However, it could be demonstrated that twitch activation is possible in bathing solutions buffered at very low free $Ca^{2+}$ concentration (Melzer, 1982*b*) and that contraction can be activated by voltage clamp depolarization in a nominally Ca-free solution containing cadmium to block $Ca^{2+}$ inward movement (Benterbusch & Melzer, 1990). This indicates that intracellular storage organelles, which are present in the form of subsarcolemmal vesicles and cisternae (Flood, 1977; Grocki, 1982), release $Ca^{2+}$ in a merely voltage-controlled manner like in skeletal muscle of vertebrates (Rios & Pizarro, 1991).

Nevertheless, $Ca^{2+}$ channels may be of importance in E–C coupling. Like in skeletal muscle a $Ca^{2+}$ channel molecule might act as a voltage sensor for the control of $Ca^{2+}$ release. In addition, the external calcium entering the cell during a depolarization might contribute to contractile activation either directly or by modulating the voltage-dependent release.

$Ca^{2+}$ currents have hitherto not been measured in *Branchiostoma* myotome cells. Here we present a first characterization of $Ca^{2+}$ channel properties in this preparation. The results show a rapid voltage-dependent activation of the $Ca^{2+}$ current and a rapid inactivation caused by the rise of the internal $Ca^{2+}$ concentration.

Some of the results have been reported in abstracts (Benterbusch & Melzer, 1988, 1989, 1990).

## METHODS

### *Preparation*

Lancelets (*Branchiostoma lanceolatum*) were obtained from the Marine Biological Laboratory at Helgoland and were kept in a sea-water aquarium at about 14 °C.

After decapitation, the ventral body wall, the viscera and the surface epithelium were removed. The preparation was transferred to an artificial sea-water solution (ASW) containing 10 mg/ml collagenase (103586, Boehringer). After incubation for 2–3 h at room temperature, notochord and nerve chord were removed from the muscle and the myotome cells were dissociated from each other by gentle shaking in enzyme-free ASW. Then suitable preparations (see the Results section) were selected for voltage clamping using the whole-cell patch clamp method.

### *Solutions*

The following solutions were used in most of the experiments.

Artificial sea-water solution (ASW) used for dissection of specimens and isolating single cells consisted of (mM): Na, 400; K, 10; Ca, 10; Mg, 50; HEPES, 10; Cl, 530; pH = 7·5.

External solution for measuring $Ca^{2+}$ inward currents (ESC) consisted of (mM): tetraethylammonium (TEA), 410; Ca, 10; Mg, 50; HEPES, 10; methane sulphonate ($CH_3SO^{3-}$), 520; tetrodotoxin (TTX), $3{\cdot}1 \times 10^{-3}$; pH = 7·5.

External solution for measuring $Ba^{2+}$ inward currents (ESB) consisted of (mM): tetraethylammonium (TEA), 410; Ba, 10; Mg, 50; HEPES, 10; Cl, 520; tetrodotoxin (TTX), $3{\cdot}1 \times 10^{-3}$; pH = 7·5.

Standard pipette solution for intracellular perfusion (IPS) consisted of (mM); Cs, 410; Na, 20; Mg, 10·3; HEPES, 10; aspartate, 420; Cl, 40; EGTA, 1; ATP, 4; pH = 7·3.

Deviations from these standard solutions are noted at appropriate places in the Results section.

The total Mg concentration in the pipette solution was chosen to obtain a free concentration of 4 mM. When the EGTA concentration in the pipette was changed to 10 mM or when EGTA was replaced by BAPTA, the total Mg concentration had to be changed in order to maintain this value. The values of total Mg were 12·3 and 11·8 mM for 10 mM-EGTA and 10 mM-BAPTA. The free concentration of $Mg^{2+}$ and $Ca^{2+}$ in the internal solutions were calculated according to Fabiato & Fabiato (1979) and Fabiato (1985) using the temperature-corrected equilibrium constants for the cation complexes of ATP, the metal ion buffers (EGTA or BAPTA) and aspartate and the program STACONS, which was kindly provided by A. Fabiato.

*Data acquisition and analysis*

For voltage clamping we used suction electrodes in the whole-cell configuration and a conventional patch clamp amplifier (EPC7, List). The electrodes were prepared from borosilicate glass (Hilgenberg, 1 mm/1·5 mm) and had tip resistances after filling with the pipette solution ranging from 1 to 3·5 MΩ.

Pulse application to the clamp circuit and simultaneous data acquisition were carried out using an IBM-AT 286-compatible microcomputer equipped with an DA–AD converter board (DT 2821-F-16SE, Data Translation) and software written in turbo-pascal. Each digital record consisted of 1024 points which contained 960 consecutive data values sampled at 5–15 kHz and information stored in a number of additional locations at the end of the record, which were used for automatic off-line analysis of experimental data files.

The holding potential was usually set at −70 or −60 mV, which is close to the resting potential recorded after establishing the whole-cell configuration. Currents were corrected for linear leak and capacitative currents by applying three to seven hyperpolarizing control pulses before and after each test pulse at intervals between 0·7 and 0·8 s. The control currents were scaled according to the ratio of test to control pulse amplitude and added to the test current record. The amplitude of the control pulses ranged between −15 and −35 mV. We verified that each individual control current matched the time course of the average and had no time-dependent component after the relaxation of the capacitative transient.

## RESULTS

*General properties of the myotome cells*

The myotomes of a lancelet are stacks of large numbers of extremely thin (1–2 μm), sheet-like cells with surface areas of up to about half a square millimetre, containing only a single layer of myofibrils. One of these myotome lamellae is shown in Fig. 1*A*. These cells can break and reseal along the boundaries of their myofibrils during the isolation procedure. This is demonstrated in Fig. 1*B*. In the example shown in this picture, a suction electrode (tip marked by the arrow) was used to establish intracellular contact with the narrow strip dangling off from the left side of the cell. By applying depolarizing pulses the strip and the lamella adjacent to it could be made to contract in synchrony, thus demonstrating an electrical connection between these two structures.

Our experiments were performed exclusively on isolated band-shaped structures, like the one shown in Fig. 1*C*, which are frequently found in cell suspensions of myotomic preparations and form at least in part by separating from the large lamellae in the way shown in Fig. 1*B*. Another part may be comprised of the superficial lamellae (Flood, 1968; Grocki, 1982), i.e. narrow cells seen in cross-sections of the trunk muscle at the outer surface of the myotomes. No data are available from the literature as to physiological differences in these two types of muscle cells and our experimental results showed no variation which would allow us to distinguish two groups of preparations.

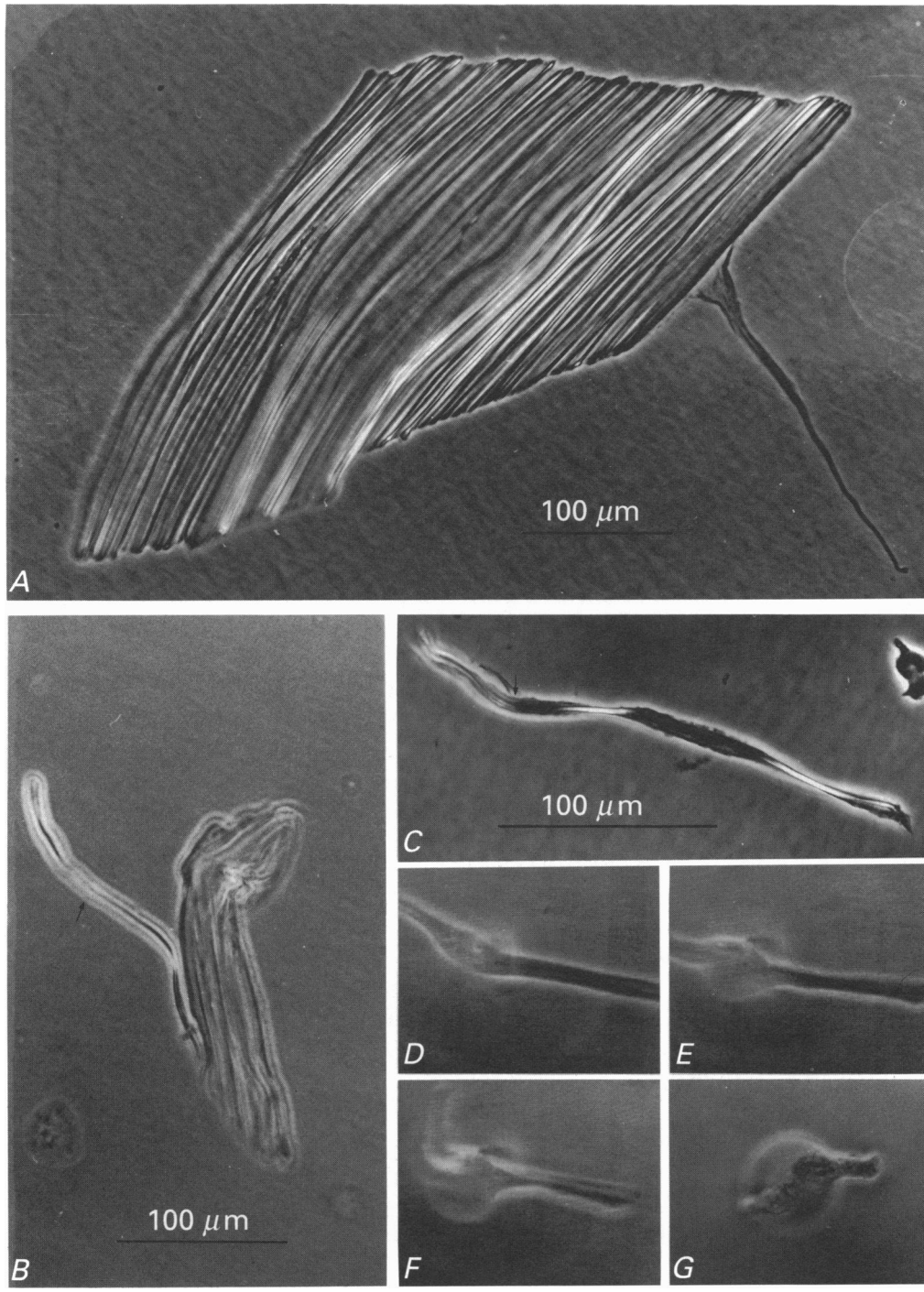


Fig. 1. Morphology of myotome lamellae (*A* and *B*) and myotome fibres (*C*). For explanation see the text. *A–C* and *G* are micrographs; *D–F* are computer reconstructions of video images recorded during experiment 185.

The width of the cell strips, which we refer to as 'myotome fibres', ranged from 7 to 12 $\mu$m. Electron micrographs have shown that the myofibrils in the myotome muscles are oval in cross-section with a width of several (often more than ten) micrometres (K. Grocki, unpublished observation). Thus the myotome fibres contain only a very small number of myofibrils and may even be single membrane-coated myotomic myofibrils.

The membrane capacitance estimated by using the capacitance compensation procedure available on the EPC-7 ranged from 22 to 96 pF. Relating these values to the microscopically determined surface areas of the fibres gave specific capacitance values between 0·7 and 1·3 $\mu$F/cm$^2$ (mean value $1{\cdot}0 \pm 0{\cdot}2$ $\mu$F/cm$^2$, $n = 48$). This is consistent with earlier current clamp measurements (Melzer, 1982*a*) and with electron microscopic studies showing that infoldings of the surface membrane are very rare (Grocki, 1982).

The great majority of the fibres maintained their shape for the duration of an experiment (generally less than 30 min). In some cases, however, a loss of structural integrity, perhaps due to a breakdown of cytoskeletal elements, occurred during perfusion. Different stages of this change are shown in Fig. 1*D–G*. Starting at the site of the pipette attachment, the growing of a vesicular structure led to transformation from the elongated band-like shape to an almost spherical morphology. In four other experiments in which a similar morphological change occurred the apparent series resistance (read from the transient compensation dials of the patch clamp amplifier) was initially 1·5–7·5 MΩ larger than the pipette resistance, which was measured before forming the patch. At the end of the transformation, the series resistance equalled the pipette resistance, indicating that an access resistance within the cell vanished during the sphere formation. A high longitudinal resistance in the fibre may hamper space clamping. One observation contradicting a significant spacial potential difference in the fibre is the fact that the measured cell capacitance (36·3 pF) did not change during the structural change illustrated in Fig. 1*D–G*. Since the main drop in the series resistance occurred early during the sphere formation we think that the access resistance is mainly located close to the tip of the pipette.

For an approximate calculation of the voltage decrement along the longitudinal axis of the fibre in the dynamic equilibrium one can use the equation for a short one-dimensional linear cable:

$$V_x/V_0 = (\cosh(L/l - x/l))/\cosh(L/l), \tag{1}$$

where $L$ is the length of the cable, $V_0$ the voltage at the site of current application, and $V_x$ the voltage at a distance $x$ from this site. The space constant $l$ can be calculated as:

$$l = \sqrt{(R_m A/R_i U)}, \tag{2}$$

where $R_m$ is the specific membrane resistance for 1 cm$^2$ of membrane area, $R_i$ the specific resistance of the myoplasm, $A$ the cross-sectional area of the fibre and $U$ its circumference. Given the width of 7–12 $\mu$m and the thickness of 1–2 $\mu$m (Grocki, 1981), $A$ ranged from 7 to $24 \times 10^{-8}$ cm$^2$ and $U$ from 16 to 28 $\mu$m. A value of 100 Ω cm was used for $R_i$ which is larger than most of the values given by Zachar (1971) for marine invertebrates. Approximate estimates of $R_m$ were taken from the slope of current–voltage relations at rest, close to the holding potential, as well as at

potentials between +20 and +50 mV after activation of the $Ca^{2+}$ current (i.e. from the ascending limb of the N-shaped $I$–$V$ relation, e.g. Fig. 6$B$). The resting resistance was about 25000 Ω $cm^2$. It dropped to about 2200 Ω $cm^2$ during maximum activation of the $Ca^{2+}$ current. For $L = 400$ μm, which corresponds to about the largest fibre

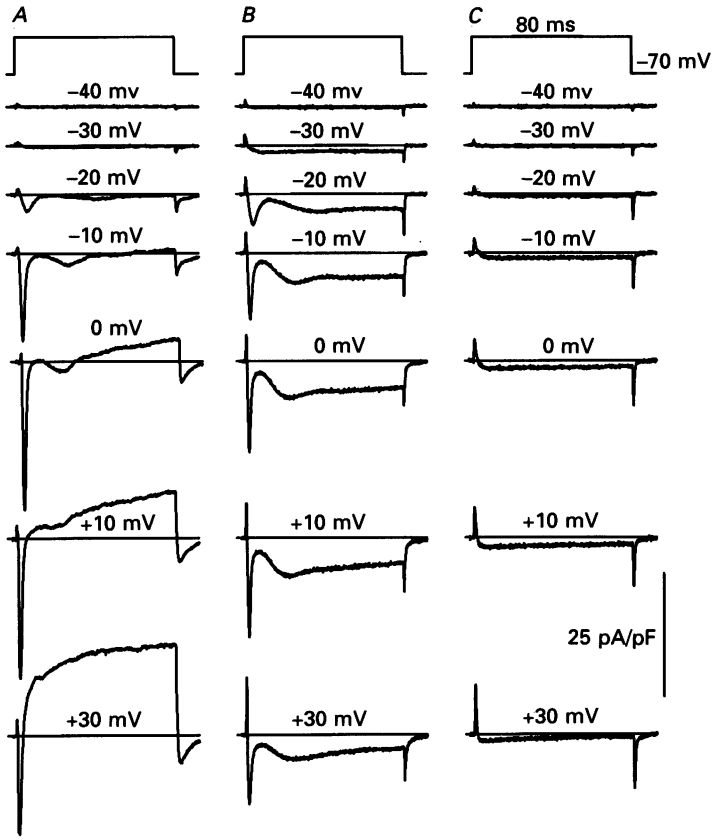


Fig. 2. Isolation of $Ca^{2+}$ inward currents in a single myotome fibre. The fibre was subjected to three different bathing solutions and in each case depolarizations to different membrane potentials were applied. $A$, solution ASW (artificial sea water); $B$, solution ESC, which blocks the currents carried by monovalent ions; $C$, solution ESC with 1 mM-cadmium. Experiment 77; membrane capacitance ($C_m$), 77 pF; holding potential (HP), −70 mV; temperature ($T$), 22·5 °C; time after establishing the whole-cell configuration ($t_{wc}$), 7 min ($A$), 14·5 min ($B$) and 21 min ($C$).

length measured in these experiments, and a location of the recording pipette in the middle of the fibre we calculated a maximum drop of the voltage at the fibre ends of between 0·97 and 1·78% at rest and between 9·7 and 17·5% during activation.

*Isolation of $Ca^{2+}$ currents*

Figure 2 shows the voltage-dependent activation of ionic currents in three different external solutions, which were applied in succession to a single myotome fibre. In Fig. 2$A$, the external solution was normal artificial sea water; since only 7 min had

elapsed after establishing the whole-cell configuration, intracellular perfusion with the pipette solution was incomplete at the time. The recordings exhibit large inward and outward currents at strong depolarizations. The records in Fig. 2*B* were obtained 7·5 min later at a more complete state of intracellular perfusion and after exchanging ASW for the standard external calcium solution (see Methods section). Net outward current is now completely suppressed even at large depolarizations (by means of TEA in the external and Cs in the internal solution) and the spike-like inward current is reduced in amplitude, reflecting a block of sodium channels by TTX and removal of external sodium. However, two distinct phases of inward current remained, which could almost completely be eliminated by adding 1 mM-cadmium (Fig. 2*C*). This indicates that the remaining inward current originates from a transmembrane $Ca^{2+}$ flux. The cadmium block could be fully reversed by changing back to the Cd-free solution (not shown).

*Two phases of inward current*

The inward current shown in Fig. 2*B* has a complex time course exhibiting a fast and a slow current maximum. The transient decline of the current might be caused by a transient outward current, which cannot be blocked by TEA. If a transient outward current were present, it would be related to the $Ca^{2+}$ current in size since we never saw a net outward transient in these solutions nor was any outward current seen in the cadmium solution.

Under the condition of advanced intracellular perfusion, an outward current would be carried predominantly by $Cs^{+}$ ions flowing through potassium channels. We therefore replaced the external TEA by 360 mM-Cs, thus drastically changing the gradient for Cs across the membrane. Figure 3 shows that this had only negligible effects on the time course and the current–voltage characteristics of the inward current components, indicating that the characteristic biphasic appearance of the inward current is associated with changes in the net $Ca^{2+}$ flux across the membrane.

The biphasic inward current (Figs 2*B* and 3) is typical of myotome cells under these conditions. This might indicate that two separate $Ca^{2+}$ currents with different time courses of activation and inactivation are present in the myotome cells. In Fig. 3, the current maxima of both components are plotted against the respective test depolarization. It shows that the two components had an indistinguishable voltage dependence of activation. Therefore, a separation of the two components by means of their voltage threshold of activation was not possible.

*Inactivation*

We tried to separate the components from each other by selectively inactivating one of them. The inactivation pulse protocol is shown in Fig. 4*A*. A conditioning pre-pulse of 10 s duration was applied from a holding potential of −70 mV to various potentials ranging from −100 to 0 mV. The long pre-pulse, whose corresponding current response is not shown in the records, was followed by a test depolarization to +15 mV. With increasingly positive values of the pre-pulse potential the amplitudes of both the fast phase and the slower phase decreased.

Figure 4*B* shows the absolute current at the end of each pre-pulse plotted against the pre-pulse potential. Up to about −40 mV, this current–voltage relation of the

total non-inactivatable current is linear. Above −40 mV, a deviation from linearity occurs, probably indicating a permanent inward current flow in this range of potentials, which is due to a small overlap between the voltage dependence of activation and inactivation.

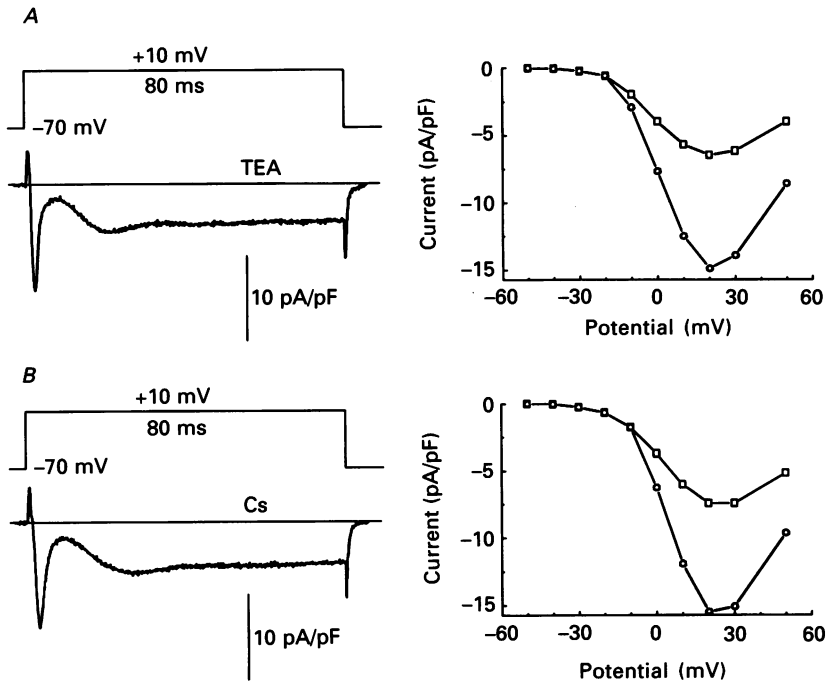


Fig. 3. Effect of substituting Cs for TEA in the external solution. *A*, left side, $Ca^{2+}$ current measured under the same conditions as in Fig. 2*B* for a 80 ms depolarization to +10 mV (solution ESC). Right side, current–voltage relationship obtained with a series of test pulses of the kind shown on the left. ○, peak values of the fast inward current component; □, peak values of the slow inward current component. *B*, same experimental procedure and corresponding plots as in *A* after 360 mM-TEA in the external bathing solution (ESC) had been replaced by an equal amount of Cs. The time course of the currents and the shape of the current–voltage relations remained virtually unchanged. Experiment 75; $C_m$, 91 pF; HP, −70 mV; *T*, 23·5 °C; $t_{wc}$, 13 min (*A*) and 23 min (*B*).

Figure 4*C* shows the amplitude of the fast (○) and the slow current component (□) as a function of the pre-pulse potential. The amplitudes were normalized to their respective values obtained at a pre-pulse potential of −100 mV. It becomes apparent that the inactivation curves of the two components are very similar. Therefore a separation of the two components by choosing a holding potential that selectively inactivates one phase was not possible.

*Fast $Ca^{2+}$-dependent inactivation*

In the experiment shown in Fig. 5, we substituted $Ba^{2+}$, for $Ca^{2+}$ as the divalent charge carrier in the external solution. The series of records shown in the left column of Fig. 5*A* demonstrates changes occurring during the solution change. When

superfusing the cell with the $Ba^{2+}$-containing solution, the decline after the rapid activation became considerably slower. This completely eliminated the biphasic character of the current. Changing back to the $Ca^{2+}$-containing solution restored the two phases of the inward current. This result suggests that the fast phase of

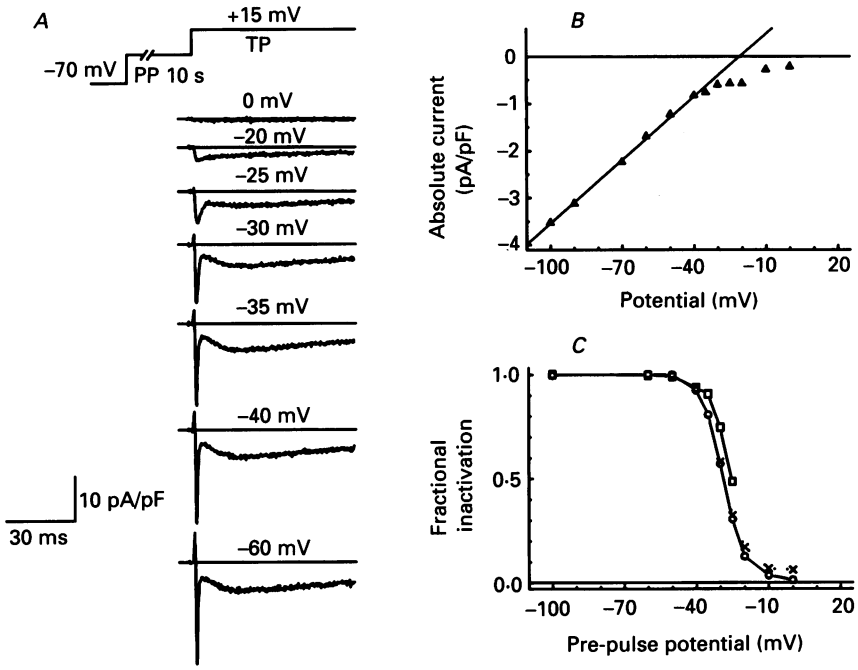


Fig. 4. Inactivation by long depolarizing pre-pulses. *A*, the current activatable by a voltage step to +15 mV (TP) was measured after a preceding 10 s period of depolarization, which caused different degrees of inactivation, depending on the potential (PP). The baseline marks the current level at the end of the pre-pulse. The different potentials used in the pre-pulse are indicated on the records. *B*, total current at the end of each 10 s pre-pulse in the experiment shown in *A*. The current–voltage relation deviates from linearity at potentials above −40 mV, probably reflecting residual inward current activation. *C*, fractional voltage dependence of inactivation. The peak of the fast (○) and slow (□) inward current component at the test pulses are plotted against the pre-pulse potentials. The amplitude was measured from the baseline before the test step. The crosses mark the fractional peak currents (fast component), taking into account the presence of the small non-zero inward current at the end of the pre-pulses above −40 mV. Experiment 92; $C_m$, 22 pF; HP, −70 mV; *T*, 24 °C; $t_{wc}$, 14 min; external solution, ESC; pipette solution, IPS.

decline is caused by rapid inactivation of the $Ca^{2+}$ conductance due to $Ca^{2+}$ ions which had entered the cell through the channel and whose function cannot be substituted by $Ba^{2+}$ ions. Furthermore, the monophasic appearance of the $Ba^{2+}$ current indicates that only one population instead of two groups of channels with different gating kinetics is involved in the $Ca^{2+}$ inward current. The second slower phase is likely to originate from a partial restoration of the channel after the rapid inactivation process. Figure 5*B* compares the initial phase of the inward current in the $Ca^{2+}$- and the $Ba^{2+}$-containing external solution at a higher time resolution. It

indicates that in $Ca^{2+}$-containing solution the activation is interrupted by the very rapid onset of the inactivation process.

Figure 6*A* compares the inward current responses in $Ca^{2+}$- and $Ba^{2+}$-containing solutions for various depolarizations from a holding potential of −70 mV. The

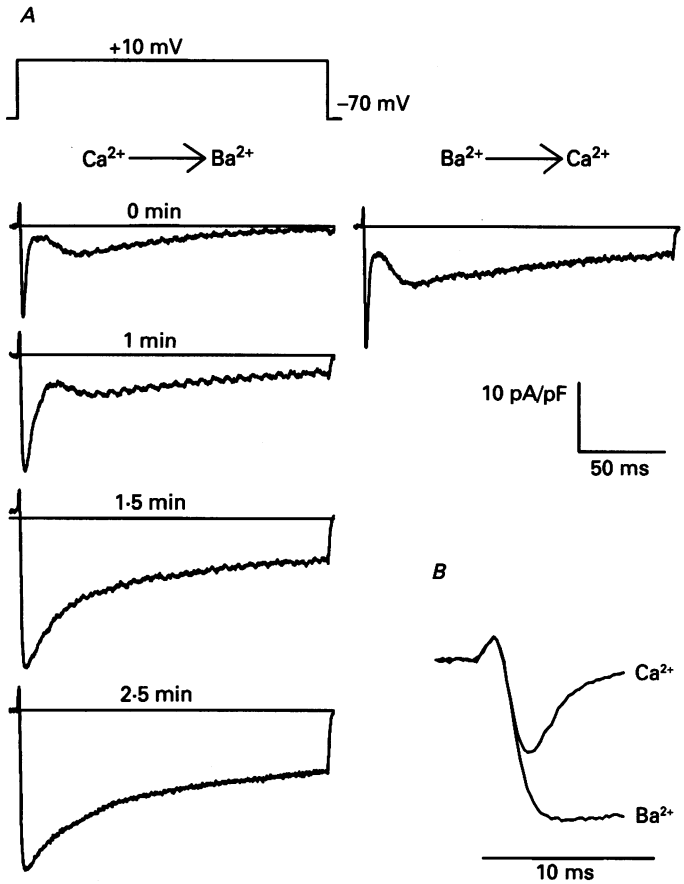


Fig. 5. Effect of substituting 10 mM-$Ba^{2+}$ for the 10 mM-$Ca^{2+}$ in the external bathing solution. *A*, the same 182 ms pulse to +10 mV was repeated at different times (indicated on the records) during the solution change. The change from solution ESC to ESB began 7·8 min ($= t_{wc}$) after establishing the whole-cell configuration. The last trace shows the result of returning to the original solution measured at $t_{wc}$ = 13 min. *B*, comparison of the initial time course of $Ca^{2+}$ and $Ba^{2+}$ current. Experiment 114; $C_m$, 41 pF; HP, −70 mV; *T*, 24 °C; pipette solution, IPS with 10 mM-EGTA.

current–voltage relations for the maximum current (Fig. 6*B*) and the corresponding activation curves (Fig. 6*C*) differ only marginally, indicating that $Ba^{2+}$ does not alter the voltage dependence of the channel activation while it has a pronounced effect on inactivation. Since initial size and activation time course of the inward currents are similar in $Ca^{2+}$- and $Ba^{2+}$-containing solutions the results rule out the possibility that the biphasic shape of the $Ca^{2+}$ current could be due to a problem of space clamping the myotome fibre.

The steady-state inactivation (Fig. 7) measured in $Ba^{2+}$, had virtually the same voltage dependence as in $Ca^{2+}$-containing solutions exhibiting 50% availability at about −30 mV. This indicates that the process responsible for the steady-state inactivation is mainly determined by cell membrane voltage and not by the nature

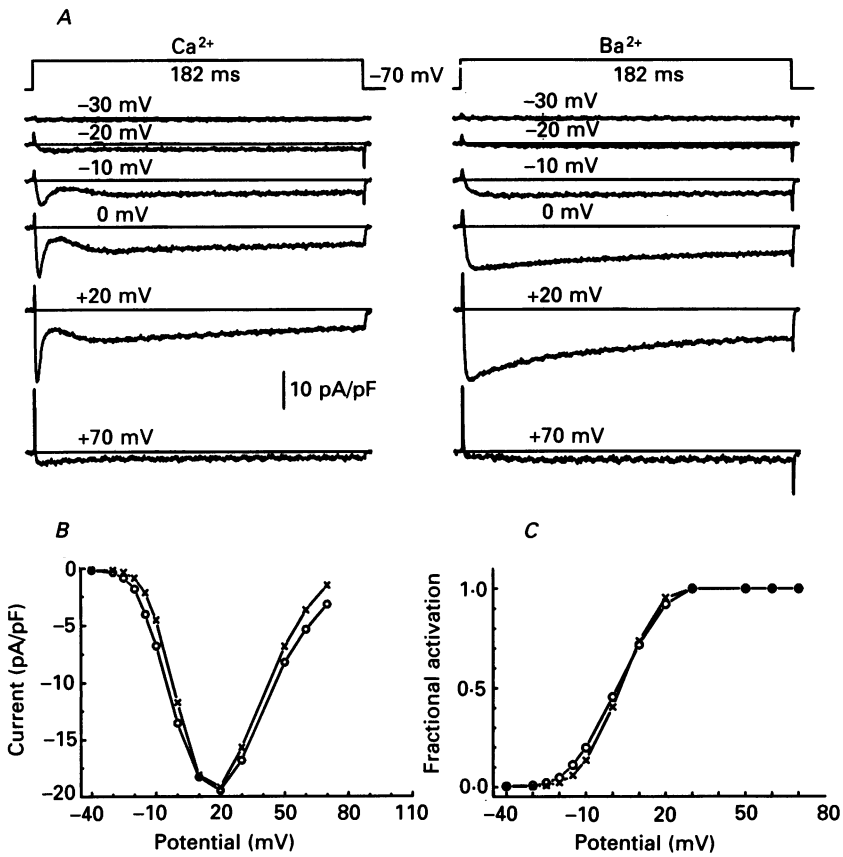


Fig. 6. Voltage dependence of $Ca^{2+}$ and $Ba^{2+}$ inward current activation. *A*, voltage-dependent activation of $Ca^{2+}$ (left) and $Ba^{2+}$ inward currents (right) measured in the same myotome fibre by applying various depolarizing pulses of 182 ms duration. The voltage during the test pulses is indicated on each record. *B*, current–voltage relations at 10 mM-external $Ca^{2+}$ and at 10 mM-external $Ba^{2+}$. Note that the plot includes more records than those shown in *A*. *C*, activation curves derived from the *I–V* relations by assuming that the maximum slope of the ascending limb represents the maximum conductance and that the open channels exhibit constant conductance over their gating range up to +50 mV. Experiment 113; $C_m$, 59 pF; HP, −70 mV; *T*, 24 °C; $t_{wc}$, 8 min (*A* left) and 29 min (*A* right); external solution, ESC (*A* left) and ESB (*A* right); pipette solution, IPS with 10 mM-EGTA.

of the ions entering the cell during activation. However, it must be noted from the traces of Fig. 6*A* that the speed of inactivation of the $Ba^{2+}$ currents also seems to depend on the size of the current. It is largest at the largest inward current amplitude (at +20 mV). Therefore inflowing $Ba^{2+}$ seems to support the inactivation process as well, even though to much less an extent than $Ca^{2+}$.

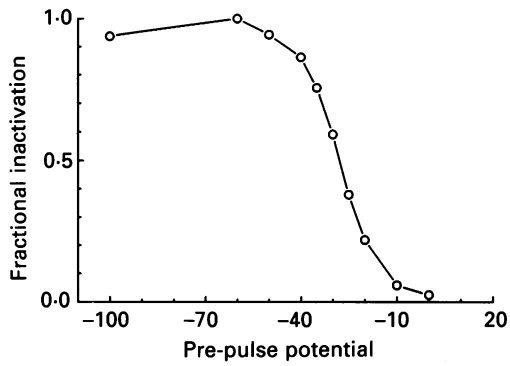


Fig. 7. Inactivation of the $Ba^{2+}$ current by long depolarizing pre-pulses. The inactivation curve was obtained by using the pulse protocol of Fig. 4*A* (records not shown). Same experiment as in Fig. 6; $t_{wc}$, 32 min.

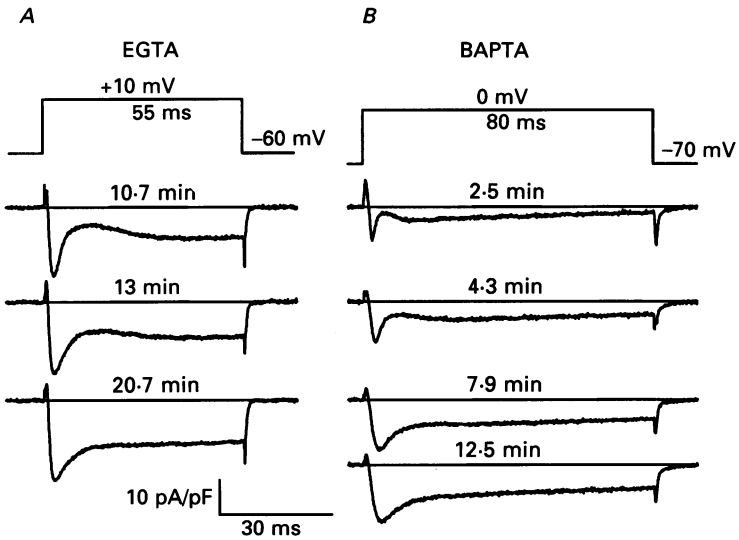


Fig. 8. Effect on $Ca^{2+}$ currents of perfusing myotome fibres with EGTA and BAPTA. The same rectangular depolarization was applied at different times ($t_{wc}$, indicated at each record) after establishing the whole-cell configuration. The pipette contained either 10 mM-EGTA (*A*) or 10 mM-BAPTA (*B*). *A*, experiment 113; $C_m$, 59 pF; HP, −60 mV; *T*, 24 °C. *B*, experiment 89; $C_m$, 46 pF; HP, −70 mV; *T*, 23 °C.

*Effects of internal $Ca^{2+}$ buffering*

The previous results indicate that a concentration increase of $Ca^{2+}$ at the cytoplasmic side of the $Ca^{2+}$ channel caused by $Ca^{2+}$ entering through the channel leads to a rapid reduction of channel conductance. Changing the extent of $Ca^{2+}$ buffering in the cytoplasm should therefore also affect fast inactivation.

In fact, we observed (Fig. 8*A*) that using 10 mM-EGTA instead of the usual 1 mM in the recording pipette changed the current in a similar way as did external $Ba^{2+}$

(Fig. 6*A*). The effect, however, could only be observed in rather long-lasting experiments, when sufficient amounts of EGTA had entered the cell by diffusion. The suppression of fast inactivation occurred considerably faster, when the chelator BAPTA instead of EGTA was present in the pipette solution (Fig. 8*B*).

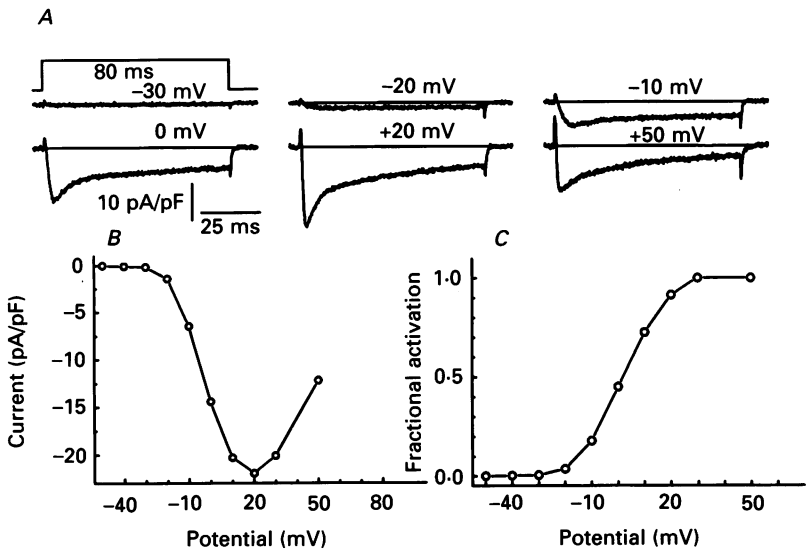


Fig. 9. Voltage-dependent activation of $Ca^{2+}$ inward currents in the presence of intracellular BAPTA. *A*, test pulses of 80 ms duration were applied after a long period (31 min) of equilibration with pipette solution IPS containing 10 mM-BAPTA instead of 1 mM-EGTA. The voltage during the test pulses is indicated on each record. *B*, voltage dependence of the peak currents obtained from the records shown in *A*. *C*, fractional activation derived from *B* in the way described in the legend of Fig. 6. Experiment 91; $C_m$, 32·5 pF; HP, −70 mV; *T*, 23 °C; $t_{wc}$, 31 min.

At physiological pH BAPTA has been reported to exhibit significantly higher on-rates for binding $Ca^{2+}$ than EGTA (Tsien, 1980). Therefore, it can be expected to buffer fast $Ca^{2+}$ transients more efficiently than the slow buffer EGTA.

Figure 9 shows the voltage dependence of $Ca^{2+}$ inward currents after 31 min of internal perfusion with a solution containing 10 mM-BAPTA. As for $Ba^{2+}$, the transformation of the biphasic to the monophasic current occurring during the perfusion with BAPTA was not accompanied by a gross change in the current–voltage relation of the peak inward current.

Even though the characteristic biphasic shape of the current has vanished in the records of Fig. 9*A*, the decline clearly exhibits two kinetically different components, with the fast one becoming less pronounced in relation to the slow one at large depolarizations. This indicates that the $Ca^{2+}$-dependent inactivation is still present. Presumably a complete removal of $Ca^{2+}$-dependent inactivation would require a very strong internal buffering by BAPTA.

The standard internal solution used in most of our experiments when recording $Ca^{2+}$ currents in the myotome cells contained 1 mM-EGTA. Under these conditions,

the slow reactivation after a strong and rapid inactivation was a typical feature of the inward current. Soon after establishing the whole-cell recording mode it could be observed in several experiments that the second component became enhanced relative to the first one with progressing diffusional exchange of the fibre lumen with

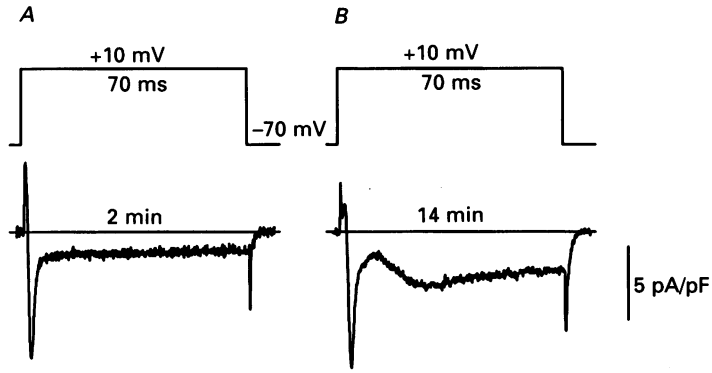


Fig. 10. Development of current reactivation with progressing intracellular perfusion. The records were obtained at 2 min and at 14 min after establishing the whole-cell configuration in a myotome fibre. 1 mM-EGTA was present in the pipette. Note the initial lack of a second phase of activation. Experiment 55; $C_m$, 60 pF; HP, −70 mV; $T$, 23 °C.

the pipette solution. This is demonstrated in Fig. 10 which shows the current at 2 min (*A*) and at 14 min (*B*) after breaking the membrane patch. In the early recording, the second phase is missing while it is pronounced in the later recording. A less pronounced slow phase was also observed in experiments with only 100–200 μM-EGTA in the recording pipette (S. Hallermann & W. Melzer, unpublished observations).

This may indicate that the artificially introduced buffer which would favour dissociation from the inactivation site augments the reactivation of the channels.

## DISCUSSION

### *Characteristics of $Ca^{2+}$ current in Branchiostoma myotome cells*

The present experiments demonstrate voltage-dependent $Ca^{2+}$ currents in *Branchiostoma* myotomes, which had been predicted by Hagiwara & Kidokoro (1971) based on action potential recordings.

Other than in skeletal muscle whose predominant $Ca^{2+}$ conductance is activated very slowly upon depolarization (Sanchez & Stefani, 1983), the myotome cells exhibit a fast voltage-activated $Ca^{2+}$ current.

We show two kinetically distinct components of $Ca^{2+}$ inward current. At first sight, this indicates the existence of two types of $Ca^{2+}$ channels but our experiments suggest that only one channel population exhibits this complex time course.

The markedly biphasic current can be explained by the fact that the $Ca^{2+}$ buffers in the artificial intracellular solutions and a rapid binding site on the channel, associated with inactivation, compete for $Ca^{2+}$ ions passing through the channel (Fig.

11). When little artificial buffering is present the current exhibits a spike and quickly drops to a much smaller level (Fig. 10*A*), due to the rapid binding of $Ca^{2+}$ to the inactivation site. On the other hand, when the $Ca^{2+}$ buffering capacity in the cell rises, dissociation from the site is enhanced, resulting in a second activation after

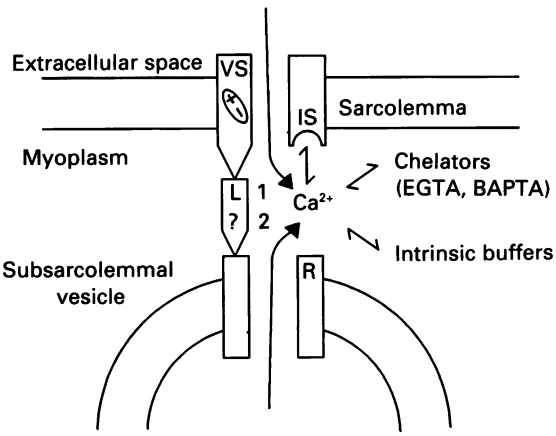


Fig. 11. $Ca^{2+}$ fluxes associated with excitation in *Branchiostoma* myotome cells. 1, $Ca^{2+}$ inward current; 2, $Ca^{2+}$ release; IS, inactivating binding site at the $Ca^{2+}$ channel; VS, voltage sensor of the $Ca^{2+}$ channel; L, hypothetical link between $Ca^{2+}$ channel and $Ca^{2+}$ release channel, which has been suggested for skeletal muscle but has not yet been established for *Branchiostoma*; *R*, $Ca^{2+}$ release channel.

rapid inactivation (Fig. 10*B*). At high intracellular buffering, the two phases merge into a single one (Fig. 7). The fast inactivation is suppressed under these conditions, because the chance is reduced that a $Ca^{2+}$ ion entering through the channel first binds to the inactivation site.

We observed a clear difference in the effect of equal concentrations of EGTA and BAPTA, which were applied via the patch pipette to fibres of comparable length and shape. It is unlikely that the stronger effect seen with BAPTA should be due to a faster diffusion of this chelator because its molecular weight is higher than that of EGTA.

The observed changes are consistent with the lower reaction rate of $Ca^{2+}$ binding to EGTA, as compared to BAPTA, which results from the fact that, at neutral pH, protons have to dissociate before $Ca^{2+}$ can bind to EGTA, while this is not the case for BAPTA (Tsien, 1980). Our results suggest that the fast and large changes of the $Ca^{2+}$ concentration, which are likely to occur at the mouth of the channel (Eckert & Chad, 1984; Smith & Augustine, 1988), can be buffered with EGTA only at significantly higher concentrations than with BAPTA.

*Possible significance for excitation–contraction coupling*

In skeletal muscle the L-type $Ca^{2+}$ channel or a protein very similar in structure (dihydropyridine receptor, DHP receptor) is involved in the control of $Ca^{2+}$ release (Pizarro, Brum, Fill, Fitts, Rodriguez, Uribe & Rios, 1988; Tanabe, Beam, Adams,

Niidome & Numa, 1990). A channel resembling the evolutionary ancestor of the L-type channel in skeletal muscle may have been preserved in the myotomes of the lancelet (Benterbusch & Melzer, 1990).

The junction between sarcolemma and subsarcolemmal vesicles contains structures similar to the 'junctional feet' in skeletal muscle (Henkart, Landis & Reese, 1976; Grocki, 1982). If the control of $Ca^{2+}$ release in myotome cells is indeed equivalent to skeletal muscle, the $Ca^{2+}$ channels investigated in this paper may likewise possess a link to the subsarcolemmal vesicles (L in Fig. 11). It is interesting to note that in the loop connecting domaines II and III on the cytoplasmic side of the $\alpha_1$-subunit of the skeletal muscle channel, a region has been identified which may comprise a $Ca^{2+}$ binding site (Tanabe, Takeshima, Mikami, Flockerzi, Takahashi, Kangawa, Kojima, Matsuo, Hirose & Numa, 1987). This loop has been shown to be essential for coupling the voltage signal of the cell membrane to the opening of the $Ca^{2+}$ release channel in the sarcoplasmic reticulum (Tanabe *et al.* 1990). One may speculate that the inactivation site of the myotome channel (IS in Fig. 11), which has been physiologically identified in the present study, may be homologous to the presumed $Ca^{2+}$ binding site on the II–III loop and might therefore be associated with the hypothetical link to the release channel. Then the unusually rapid $Ca^{2+}$-dependent inactivation of the myotome $Ca^{2+}$ current could result from an impairment of diffusional spread of inflowing $Ca^{2+}$ caused by the large extramembranal portion ('foot') of the $Ca^{2+}$ release channel (Takeshima, Nishimura, Matsumoto, Ishida, Kangawa, Minamino, Matsuo, Ueda, Hanaoka, Hirose & Numa, 1989). Vice versa, $Ca^{2+}$ release from the subsarcolemmal vesicles may contribute to the inactivation of the $Ca^{2+}$ channel. In future experiments, it will be necessary to test whether events in excitation–contraction coupling are in fact correlated with the $Ca^{2+}$ channel function in *Branchiostoma*.

We wish to thank Drs H. Ch. Lüttgau, D. Feldmeyer, R. Thieleczek and F. Herberg for helpful discussions at different stages of the work, W. Grabowski, P. Greger and W. Ihm for support in setting up the equipment, and Mrs B. Pohl and Mrs H. Jung for technical help. We also thank Ms E. Linnepe for suggestions concerning the manuscript and we are grateful to Mr R. Schwalm for doing an excellent job in developing the data acquisition system. This work was supported by a grant from the Deutsche Forschungsgemeinschaft (FG Konzell) and by a scholarship from the Studienstiftung des Deutschen Volkes to R. Benterbusch.

## REFERENCES

ASHLEY, C. C., MULLIGAN, I. P. & LEA, T. J. (1991). $Ca^{2+}$ and activation mechanisms in skeletal muscle. *Quarterly Reviews of Biophysics* **24**, 1–73.

BEAN, B. P. (1986). Calcium channels in skeletal muscle: what do they do? *Trends in Neurosciences* **9**, 535–536.

BENTERBUSCH, R. & MELZER, W. (1988). Ca currents and excitation–contraction coupling in muscle cells of the lancelet (*Branchiostoma lanceolatum*). *Pflügers Archiv* **411**, suppl. 1, R190 (368).

BENTERBUSCH, R. & MELZER, W. (1989). Modification of Ca inward current components in isolated myotome cells of *Branchiostoma* by use of intracellular fast Ca buffers. *Journal of Physiology* **415**, 129*P*.

BENTERBUSCH, P. & MELZER, W. (1990). Voltage-dependent contractile activation and intramembrane charge movements in myotome cells of the lancelet (*Branchiostoma lanceolatum*). *Pflügers Archiv* **415**, suppl. 1, R70 (256).

ECKERT, R. & CHAD, J. E. (1984). Inactivation of Ca channels. *Progress in Biophysics and Molecular Biology* **44**, 215–267.

FABIATO, A. (1985). Time and calcium dependence of activation and inactivation of calcium-induced release of calcium from the sarcoplasmic reticulum of a skinned canine cardiac Purkinje cell. *Journal of General Physiology* **85**, 247–289.

FABIATO, A. & FABIATO, F. (1979). Calculator programs for computing the composition of the solutions containing multiple metals and ligands used for experiments in skinned muscle cells. *Journal de Physiologie* **75**, 463–505.

FLOOD, P. R. (1977). The sarcoplasmic reticulum and associated plasma membrane of trunk muscle lamellae in *Branchiostoma lanceolatum* (Pallas). *Cell and Tissue Research* **181**, 169–196.

FLOOD, P. R. (1968). Structure of the segmental trunk muscle in *Amphioxus*. *Zeitschrift für Zellforschung* **84**, 389–416.

FRANZ, V. (1927). Morphologie der Akranier. *Ergebnisse der Anatomie und Entwicklungsgeschichte* **27**, 464.

GROCKI, K. (1982). The fine structure of the deep muscle lamellae and their sarcoplasmic reticulum in *Branchiostoma lanceolatum*. *European Journal of Cell Biology* **28**, 202–212.

HAGIWARA, S., HENKART, M. P. & KIDOKORO, Y. (1971). Excitation–contraction coupling in *Amphioxus* muscle cells. *Journal of Physiology* **219**, 233–251.

HAGIWARA, S. & KIDOKORO, Y. (1971). Na and Ca components of action potential in *Amphioxus* muscle cells. *Journal of Physiology* **219**, 217–232.

HENKART, M., LANDIS, D. M. D. & REESE, T. S. (1976). Similarity of junctions between plasma membranes and endoplasmic reticulum in muscle and neurons. *Journal of Cell Biology* **70**, 338–347.

LAMB, G. D. (1991). $Ca^{2+}$ channels or voltage sensors? *Nature* **352**, 113.

MELZER, W. (1982*a*). Electrical membrane properties of the muscle lamellae in *Branchiostoma* myotomes. *European Journal of Cell Biology* **20**, 213–218.

MELZER, W. (1982*b*). Twitch activation in $Ca^{2+}$-free solutions in the myotomes of the lancelet (*Branchiostoma lanceolatum*). *European Journal of Cell Biology* **28**, 219–225.

PIZARRO, G., BRUM, G., FILL, M., FITTS, R., RODRIGUEZ, M., URIBE, I. & RIOS, E. (1988). The voltage sensor of skeletal muscle excitation–contraction coupling: A comparison with $Ca^{2+}$ channels. In *The Calcium Channel: Structure, Function and Implications*, ed. MORAD, M., NAYLER, W., KAZDA, S. & SCHRAMM, M., pp. 138–156. Springer-Verlag, Berlin.

RIOS, E. & PIZARRO, G. (1991). Voltage sensor of excitation–contraction coupling in skeletal muscle. *Physiological Reviews* **71**, 849–907.

SANCHEZ, J. A. & STEFANI, E. (1983). Kinetic properties of calcium channels of twitch muscle fibres of the frog. *Journal of Physiology* **337**, 1–17.

SMITH, S. J. & AUGUSTINE, G. J. (1988.). Calcium ions, active zones and synaptic transmitter release. *Trends in Neurosciences* **11**, 458–464.

TAKESHIMA, H., NISHIMURA, S., MATSUMOTO, T., ISHIDA, H., KANGAWA, K., MINAMINO, N., MATSUO, H., UEDA, M., HANAOKA, M., HIROSE, T. & NUMA, S. (1989). Primary structure and expression from complementary DNA of skeletal muscle ryanodine receptor. *Nature* **339**, 439–445.

TANABE, T., BEAM, K. G., ADAMS, B. A., NIIDOME, T. & NUMA, S. (1990). Regions of the skeletal muscle dihydropyridine receptor critical for excitation–contraction coupling. *Nature* **346**, 567–569.

TANABE, T., TAKESHIMA, H., MIKAMI, A., FLOCKERZI, V., TAKAHASHI, H., KANGAWA, K., KOJIMA, M., MATSUO, H., HIROE, T. & NUMA, S. (1987). Primary structure of the receptor for calcium channel blockers from skeletal muscle. *Nature* **328**, 313–318.

TSIEN, R. Y. (1980). New calcium indicators and buffers with high selectivity against magnesium and protons: Design, synthesis, and properties of prototype structures. *Biochemical Journal* **19**, 2396–2404.

ZACHAR, J. (1971). *Electrogenesis and Contractility in Skeletal Muscle Cells*. Publishing House of the Slovak Academy of Sciences, Bratislava, CSSR.